Korean J. Chem. Eng., 34(6), 1801-1812 (2017)
DOI: 10.1007/s11814-017-0075-4

pISSN: 0256-1115
eISSN: 1975-7220

Silver nanoparticle loaded silica adsorbent for wastewater treatment

Vaidyanathan Thamilselvi and Kuravappulam Vedhaiyan Radha†

Bioproducts Lab., Department of Chemical Engineering, A.C. Tech, Anna University, Chennai-25, India
(*Received 10 August 2016 • accepted 16 March 2017*)

Abstract−Our aim was to prepare silver nanoparticle loaded silica adsorbent for the removal of pollutants and pathogens in wastewater. The pathogens were inactivated by silver nanoparticles loaded with silica by wet impregnation method. Fourier transform infrared spectroscopy, energy dispersive X-ray spectroscopy, and X-ray Diffraction studies confirmed the silver nanoparticle loaded on silica. Inductively coupled plasma atomic emission spectroscopy showed 0.6 mg/g silver nanoparticle in the prepared adsorbent. The prepared adsorbent has potential against *Escherichia coli* and was described through Chick, Chick-Watson and Homs inactivation kinetic models. Five-hundred (500) ppm concentration of the prepared adsorbent showed complete inhibition with the shouldering or lag curve of inactivation and the k′ values of 0.019 min^{-1}. After treatment, tannery, dairy and canteen effluents showed significant COD reduction with maximum adsorption capacity of 145, 142 and 69 mg/g visa versa. Regeneration of the spent adsorbent used alkali washing and reused up to three cycles.

Keywords: Amine Functionalized Silica, Adsorption, Impregnation, Inactivation, Isotherm

INTRODUCTION

Wastewater disposed from industrial sectors constitutes organic and inorganic contaminants and microbial contaminants [1]. This contaminated water poses a health risk to human beings [2]. Several physicochemical techniques have been used for the treatment of wastewater and proven that adsorption is a successful method [3]. Advances in nanotechnology, which is an emerging field, have led to new adsorbent materials for efficient water treatment. Adsorptive removal of pollutants from wastewater using nanoparticles have received much consideration due to the large surface area and an availability of active sites. The limitations of using nanomaterials for water treatment are an aggregation of nanomaterials and biofouling. This can be overcome by coating the antibacterial agents for disinfection on the adsorbent. These disinfectant coated adsorbent materials are stable and effective in water treatment systems. While the conventional disinfectants of chlorites and chloramines have limitations such as high dosage and carcinogenic byproducts, silver nanoparticles are a good alternative and have proven to be an effective disinfectant for water treatment [4].

Silver nanoparticles have been reported for their bactericidal effect and usefulness in the range of products from pharmaceutical, textile, and paint industries [4]. Due to the higher cost of commercial silver nanoparticles, the synthesis of silver nanoparticles is considered. The physical and chemical synthesis of silver nanoparticle has the disadvantages of emission of the toxicants, heat and high energy consumption. Hence, the environmental friendly biological mode of silver nanoparticle is widely accepted. The biosynthesized silver nanoparticle is reported to be stable, biocompatible and non-toxic to the human epidermal karatinocytes [5]. The lower concentration of silver nanoparticle from 2 ppm to 4 ppm is nontoxic to human cells (HEK 293) and toxic to bacterial cells [6]. Moreover, silver nanoparticle can easily load within the porous substrates such as mesoporus silica, zeolite, ceramics [7], activated carbon [8], polyurethane, and chitosan [9]. These silver nanoparticle loaded adsorbents are reported as a good alternative for water purification filters. Silver nanoparticle acts as a disinfectant that does not alter the adsorption capacity and improves the ability of an adsorbent [10].

The choice of sorptive material for the loading of silver nanoparticles as nonporous material is advantageous, in order to avoid pore diffusion and decreased efficiency. Silica is a nonporous material that captures contaminants [11] and has mechanical resistance [12]. Silica can be used as a carrier for silver nanoparticles and the silica-silver composites are thermally stable [13]. Strong binding of silver nanoparticles onto the silica surface is made by the functionalization of silica with thiol or amino group. The dry method of impregnation of silica with silver nanoparticle is advantageous and cost effective, overcoming the limitation of high expenditure by solvent method. Similar chemical preparation of silver silica composite was reported earlier [14]; moreover, the silver loading on the adsorptive surface does not alter adsorption efficiency [10]. The advantage of those organometallic nanoparticles is that they are firm and not decomposable.

In this study we prepared the silver nanoparticle loaded silica adsorbent for the treatment of wastewater. The biosynthesis of silver nanoparticle and loading on silica reduces the toxic byproducts of chemical reactants and is easily maintainable. The silver resistant bacterial strain of *Pseudomonas putida* NCIM 2650 was used for the synthesis of silver nanoparticle. The prepared silver nanoparticle have potent antibacterial activity [15]. The biosynthesized silver nanoparticle was loaded on the amine functionalized silica and used as a potential adsorbent for the application of treating indus-

†To whom correspondence should be addressed.
E-mail: thamilselvipalanivel@yahoo.in

trial disposal. Furthermore, the properties of an adsorbent have been studied by the COD reduction against effluent samples. The most common organic contaminants from these effluents are dye molecules, carbohydrates, proteins and fats, etc., were reduced by the treatment of using silver nanoparticles loaded silica. The antibacterial efficiency of an adsorbent was examined against *E. coli*.

MATERIALS AND METHODS

1. Wastewater and Materials

The analytical by pure grade chemicals of silver nitrate, tryptone, yeast extract, sodium chloride, sodium hydroxide, agar, silica, 3-aminopropyl triethoxy silane (3-APTES), concentrated nitric acid, concentrated sulfuric acid, pssium dichromate, silver sulphate, ferrous ammonium sulfate, mercuric sulfate and ferroin indicator were procured from Sisco Research Laboratory chemicals, Chennai, India. Silver nanoparticle obtained from the biosynthesis of *Pseudomonas putida* NCIM 2650.

2. Organism and Culture Maintenance

The inactivation experiments used gram negative bacterial strains of *E. coli* NCIM 2685, purchased from the National Collection of Industrial Microorganisms (NCIM), Pune, India. The culture was stored at 4 °C in nutrient agar slants. The culture was maintained by continuous sub-culturing every 14 days.

3. Preparation of an Adsorbent

For the preparation of the adsorbent the procedure described by Quang et al. [14] was followed with modification: In a 500 mL beaker 100 g of silica gel was added to 40 ml of 3-aminopropyl triethoxy silane (3-APTES) in 110 mL of 4% of nitric acid. The mixture was immediately stirred using a glass rod for 2 min and covered with aluminum foil to avoid evaporation. The amine functionalized silica was dried in an oven at 80 °C for 3 h, then washed with distilled water and further dried at 100 °C for 5 h. The amine functionalized silica (100 g) was then added to 300 ml of biosynthesized silver nanoparticle (0.330 mg/L) from *Pseudomonas putida* NCIM 2560 [15]. The mixture was stirred for 4 h. The resultant silver nanoparticle loaded silica, was washed with distilled water for the removal of unbound silver ions and the samples were dried at 100 °C for 3 h and stored in an airtight container.

4. Characterization Studies of a Prepared Adsorbent

The UV-spectroscopy (T 90+ UV/Vis SPEC PG Instruments Ltd.) of the prepared adsorbent was analyzed at room temperature in an automated wavelength range of 200 to 600 nm. The functional groups present in the prepared adsorbent were recorded by Fourier transform infrared spectroscopy (FTIR - Perkin Elmer Spectrum 400) using KBr pellets in the frequency range of 4,000 to 400 cm^{-1}, and at a resolution of 4 cm^{-1}. The morphological and elemental studies of the adsorbent were analyzed through scanning electron microscopy and energy dispersive X-ray spectroscopy (Carl Zeiss MA15/EVO 18). X-ray diffraction (XRD 6000 Shimazu) analysis of silver nanoparticle on silica was operating at 40 kV with the wavelength of 1.54 A°. The silver nanoparticle on silica was quantified using inductively coupled plasma optical emission spectrometry (Perkin Elmer Optima 5300 DV) and atomic absorption spectrometry. The physical nature of the adsorbent, BET surface area and pore size were analyzed using nitrogen adsorption instrument (Quantachrome Instruments, version 5.02).

5. *E. coli* Inactivation Using Silver Nanoparticle Loaded Silica

To study the influence of silver nanoparticle loaded silica on the inactivation of bacteria, *E. coli* NCIM 2685 of ~10^8 CFU/mL was cultured in L.B broth supplemented with silver nanoparticle loaded silica in concentrations of 100-500 ppm. Silver nanoparticle loaded silica free LB broth cultured under the same condition was used as a control. The culture flasks were incubated in an orbital shaker at room temperature. The growth and bacterial concentration were determined by measuring $O.D_{600}$ at regular intervals of 60 min. The viable cell count was performed by withdrawing the samples (100 μL) from the culture flash at a time interval of 60 min. The samples were diluted and spread on the agar plates, then the viable colonies were counted after 24 h of incubation.

Inactivation of *E. coli* NCIM 2685 was determined by calculating viable cell count CFU/mL after a period of time, expressed as % of reduction as given below [16]:

$$\text{Reduction } \% = \frac{(N_0 - N_t)}{N_0} \times 100 \quad (1)$$

where N_t is the number of CFU/mL at any defined time, and N_0 is the initial number of CFU/mL. The Chick, Chick-Watson and Homs are the well-known disinfection kinetic models that were considered, in order to describe the inactivation of *E. coli* NCIM 2685 (Table 1).

6. Batch Adsorption Studies for COD Reduction Using Silver Nanoparticle Loaded Silica

Wastewater samples, dairy effluent from Sholinganallur Aavin, tannery effluent from Avadi Tannery plant and canteen effluent from the Anna University Canteen, Chennai, India were obtained. Wastewater (tannery, dairy and canteen) treatment studies were carried out in batch mode at room temperature in a 1,000 mL conical flask, maintained in constant shaking (120 rpm). The parameters influencing the adsorption process, such as adsorbent dosage (20, 40, 60, 80, 100 g/L), and contact time (30-300 min), were studied by varying one parameter and keeping the other two as constant. The samples were withdrawn at regular time interval of 30 min; the COD reduction was measured according to standard method [17].

The COD removal efficiency of silver nanoparticle loaded silica was calculated using the given equation [18]:

$$q_e = \frac{(C_0 - C_e)V}{M} \quad (2)$$

where q_e (mg/g) is the equilibrium adsorption capacity, C_0 and C_e are the initial and equilibrium COD concentration (mg/L), V is the

Table 1. Inactivation kinetic models against *E. coli* NCIM 2685

Inactivation kinetic model	Non-linear equation	Reference
Chick	$\ln\frac{N_t}{N_0} = -kt$	[16]
Chick-Watson	$\ln\frac{N_t}{N_0} = -k'C^n t$	[44]
Homs	$\ln\frac{N_t}{N_0} = -k'C^n t^m$	[45]

Table 2. Adsorption isotherm and kinetic models

Adsorption isotherm model	Non-linear equation	Reference
Langmuir	$q_e = \frac{q_0 b C_e}{1 + b C_e}$	[46]
Freundlich	$q_e = K_F C_e^{1/n}$	[47]
Redlich-Peterson	$q_e = \frac{K_R C_e}{1 + \alpha_R C_e^{\beta}}$	[48]
Sips	$q_e = \frac{q_m (k_s C_e)^{1/n}}{1 + (k_s C_e)^{1/n}}$	[49]
Kinetic model	**Linear equation**	**Reference**
Zero order	$C_t = C_i - Kt$	[50]
First-order	$\ln C = \ln C_i - K_1 t$	[50]
Second-order	$\frac{1}{C_t} = \frac{1}{C_i} + K_2 t$	[50]
Pseudo-first order equation	$\log(q_e - q_t) = \log(q_e) - \frac{K_{1p} t}{2.303}$	[51]
Pseudo-Second order	$\frac{t}{q_t} = \frac{1}{K_{2p} q^2} + \frac{1}{q_e} t$	[51]

volume (mL) of the sample solution taken for COD analysis, and M is the weight of the adsorbent (mg). The equilibrium experimental data were analyzed using Langmuir, Freundlich, Redlich Peterson and Sips isotherm models using the software MATLAB version R2010 [19]. Kinetic models, zero-order, first-order, second-order, pseudo-first-order and pseudo-second-order were used to analyze the COD removal as described in Table 2.

7. Quantification of Silver in the Treated Water and Regeneration of Spent Silver Nanoparticle Loaded Silica

The treated samples of tannery, dairy and canteen effluent were analyzed by inductively coupled plasma optical emission spectrometry (ICP-OES) for quantifying silver traces in the treated water. The exhausted silver nanoparticle loaded silica was regenerated and reused after alkali wash. For desorbing the impurities from the adsorbent, NaOH was preferred, and it was reported in effective removal of natural oil, fats, waxes, surfactant and suspended impurities [20]. 1 g of exhausted adsorbent was washed with the different concentration of sodium hydroxide (0.05, 0.1 and 0.15 M) and kept in a shaker (120 rpm) for 3 h. The alkali washed adsorbent was filtered and rinsed several times with distilled water until the pH of 7, followed by drying in a hot air oven at 100 °C for 24 h. Finally, the regenerated adsorbent was reused for COD removal from tannery, dairy and canteen effluents at an optimum adsorption conditions.

The growth inhibition studies of the prepared adsorbent and the spent adsorbent up to three cycles were analyzed by pour plate experiment. 1 mL of serially diluted *E. coli* (10^{-5}) culture was poured into a sterile petri plate and 15 mL of 500 ppm silver nanoparticle loaded silica supplemented agar medium was added. The control experiment was performed with the silica supplemented agar medium. The petri plates were allowed for solidification and incubated, then the viable count was observed after 24 h.

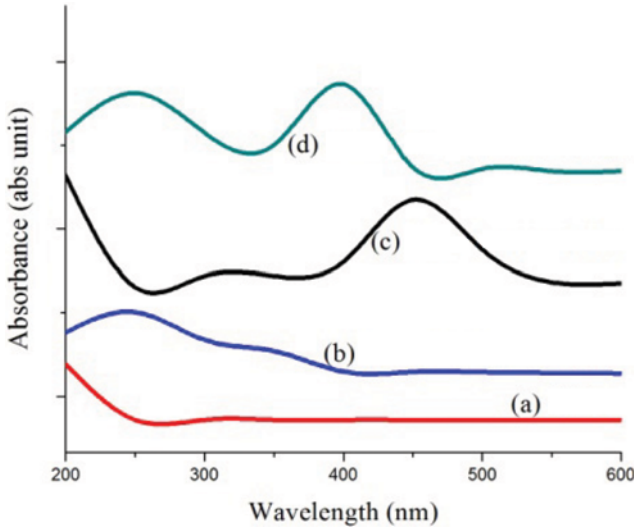

Fig. 1. UV spectra of (a) Silica, (b) Amine functionalized silica, (c) Silver nanoparticle, and (d) Silver nanoparticle loaded silica.

RESULTS AND DISCUSSION

1. Characterization of Silver Nanoparticle Loaded Silica

The silver nanoparticle loaded on the surface of amine functionalized silica was determined by UV-Spectroscopy as shown in Fig. 1. The spectra show that there were no peaks observed for silica, while the silver nanoparticle loaded silica showed absorption peaks at 250 nm and 400 nm, which confirms the presence of amino group and silver nanoparticle. The presence of amino group was indicated by the absorption peak in the near UV region ranges from 240 nm to 300 nm [19,54]. The preliminary studies of silver nanoparticle was reported with the characteristic surface plasmon resonance (SPR) band, wavelength ranges from 400 nm to 530 nm [55]. Previous studies showed a peak at 415 nm for silver nanoparticle incorporated silica, indicating the presence of silver and no peaks

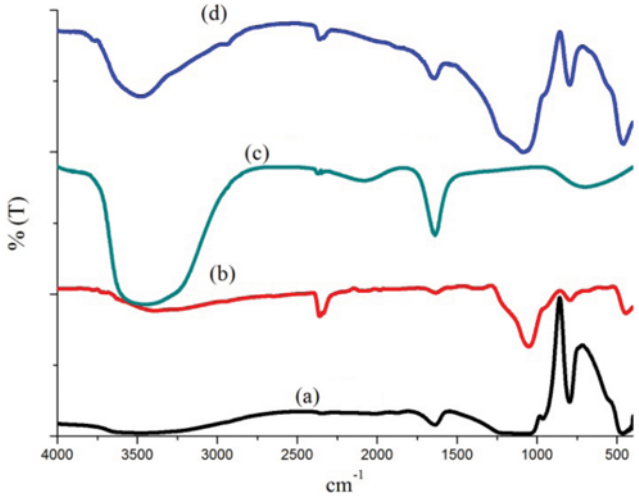

Fig. 2. FTIR spectra of (a) Silica, (b) Amine functionalized silica, (c) Silver nanoparticle and (d) Silver nanoparticle loaded silica.

for silica [14]. Similarly, the UV-absorption bands around 400 nm were attributed for the surface plasmon resonance of the metal nanoparticle [21,22].

The FTIR spectra of silver nanoparticle loaded silica are shown in Fig. 2. The silica spectrum with broad band at 3,500 and 1,630 cm^{-1} is assigned to the vibration of -OH groups. The absorption band at 1,040 and 800 cm^{-1} corresponds to Si-O-Si stretching vibrations. The absorption band at 900 cm^{-1} is due to the Si-OH bending vibration. These bands indicate the hydrogen bonding forms the silanol groups (Fig. 2(a)). Fig. 2(b) shows the FTIR spectrum of amine functionalized silver nanoparticle; the band at 900 cm^{-1} corresponding to Si-OH stretching vibration was considerably reduced after being functionalized with 3-APTES, due to the condensation of silanol group. The absorption peak at 1,040 cm^{-1} was assigned to Si-O-Si asymmetric stretching vibration. A new band detected at 2,400 cm^{-1} was assigned to the carbonyl group, indicating the successful grafting of amino functional group [14]. Fig. 2(c) shows the absorption spectrum of silver nanoparticle; the significant bands at 3,400 and 1,640 cm^{-1} were attributed to -OH stretching vibrations and primary amides, indicating the stabilization of silver nanoparticle by bacterial protein molecules [15]. Fig. 2(d) shows the absorption spectrum of silver nanoparticle loaded silica; the band at 3,500 cm^{-1} corresponds to -OH stretching vibration. The bands located at 2,400 cm^{-1}, 1,040 and 1,640 cm^{-1} correspond to the carbonyl group, Si-O-Si stretching vibrations and the primary amide group, respectively. The band at 900 cm^{-1} was assigned to the Si-OH stretching vibration. These absorption peaks indicate that functionalization of the amino functional group and loaded silver nanoparticle on the silica surface by electrostatic bond formed between the silver nanoparticle and the amino group of functionalized silica. This may be due to the strongly attached amino group of amine functionalized silica to the silver nanoparticle through two major bonding factors, which are anchoring bond and non conventional hydrogen bonds [52].

The surface morphology of silica and silver nanoparticle loaded silica was analyzed by SEM, as shown in Fig. 3. SEM micrograph of silica is shown in Fig. 3(a) with rough and irregular nature. The silver nanoparticle loaded silica (Fig. 3(b)) shows the silver nano-

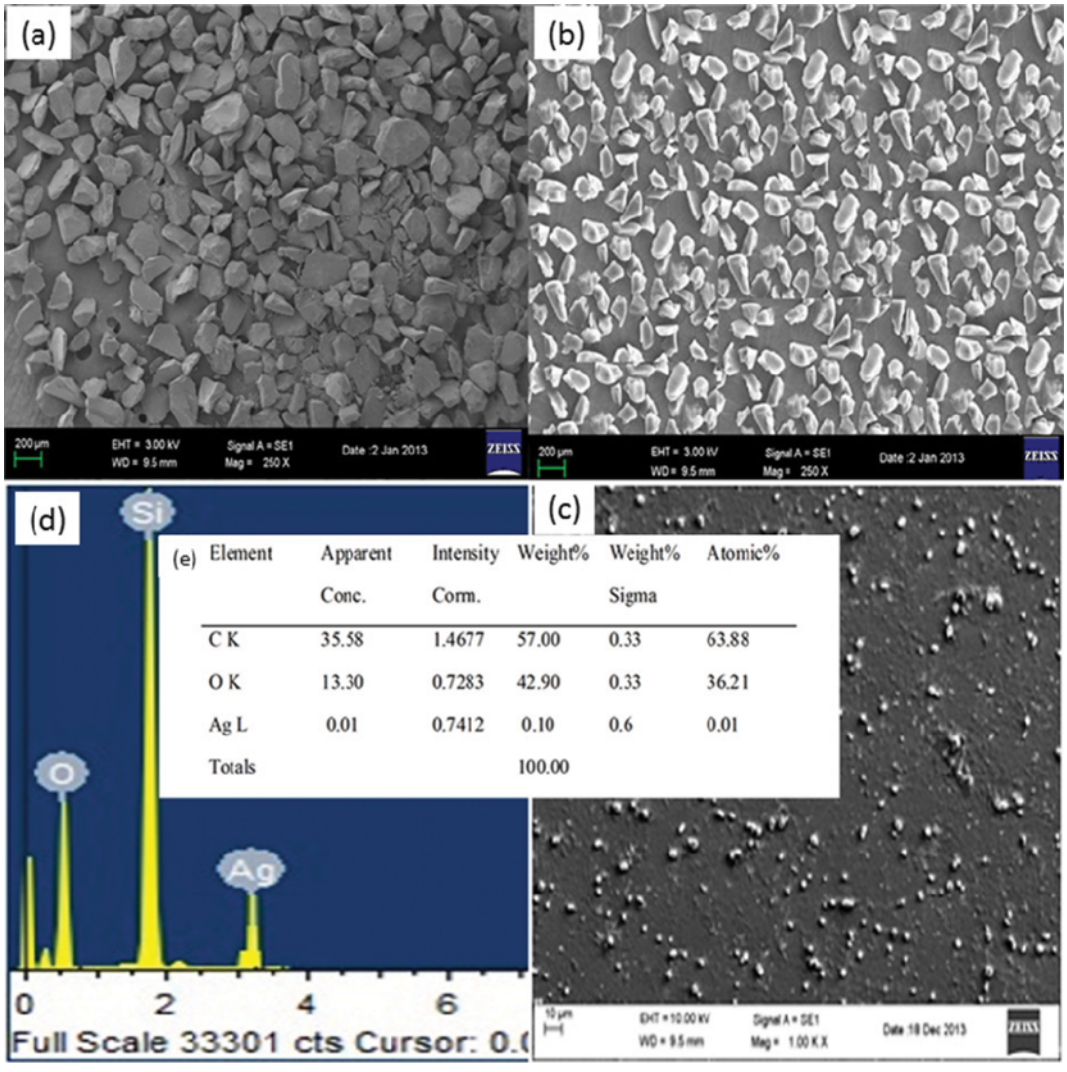

Element	Apparent Conc.	Intensity Corrn.	Weight%	Weight% Sigma	Atomic%
C K	35.58	1.4677	57.00	0.33	63.88
O K	13.30	0.7283	42.90	0.33	36.21
Ag L	0.01	0.7412	0.10	0.6	0.01
Totals			100.00		

Fig. 3. SEM images of (a) Silica (b) silver nanoparticle loaded silica, (c) silver nanoparticle loaded silica (100 KX), (d) EDX spectra of silver nanoparticle loaded silica, (e) EDX table.

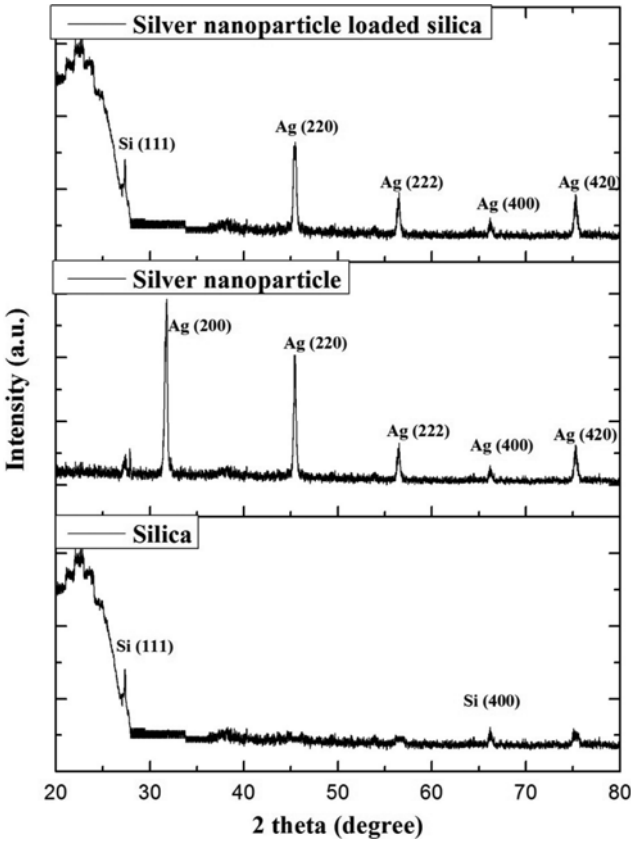

Fig. 4. XRD patterns of the prepared materials.

particle coated on silica surface, and the texture was significantly modified as porous and crystalline nature. Fig. 3(c) shows the silver nanoparticle loaded silica at magnification of 100KX. The EDX elemental analysis of silver nanoparticle loaded silica was observed with a substantial peak for silver content of 0.6 weight % (Fig. 3(d)). SEM-EDX analysis by Li et al. [12] reported the presence of 0.57% silver on silica surface by chemical method.

The XRD patterns of silica, silver nanoparticle and silver nanoparticle loaded corncob are shown in Fig. 4. In the silver nanoparticle loaded silica, the broadened diffraction peak recorded at 2θ value of 27.37° corresponds to the plane (111) of amorphous silica and the value of 45.48°, 56.51°, 66.23° and 75.31° corresponds to the plane (220), (222), (400) and (420) of crystalline cubic silver nanoparticle. The average crystalline size of silver nanoparticle calculated using Scherrer's equation was 32 nm. These results confirmed the silver nanoparticle loaded on silica.

The ICP-OES analysis of silver nanoparticle loaded silica shows 0.6 (±0.2) mg/g of silver nanoparticle loaded on the silica surface. The AAS analysis confirmed 0.7% of silver nanoparticle on silica. These results confirm the surface loading of silver nanoparticle on

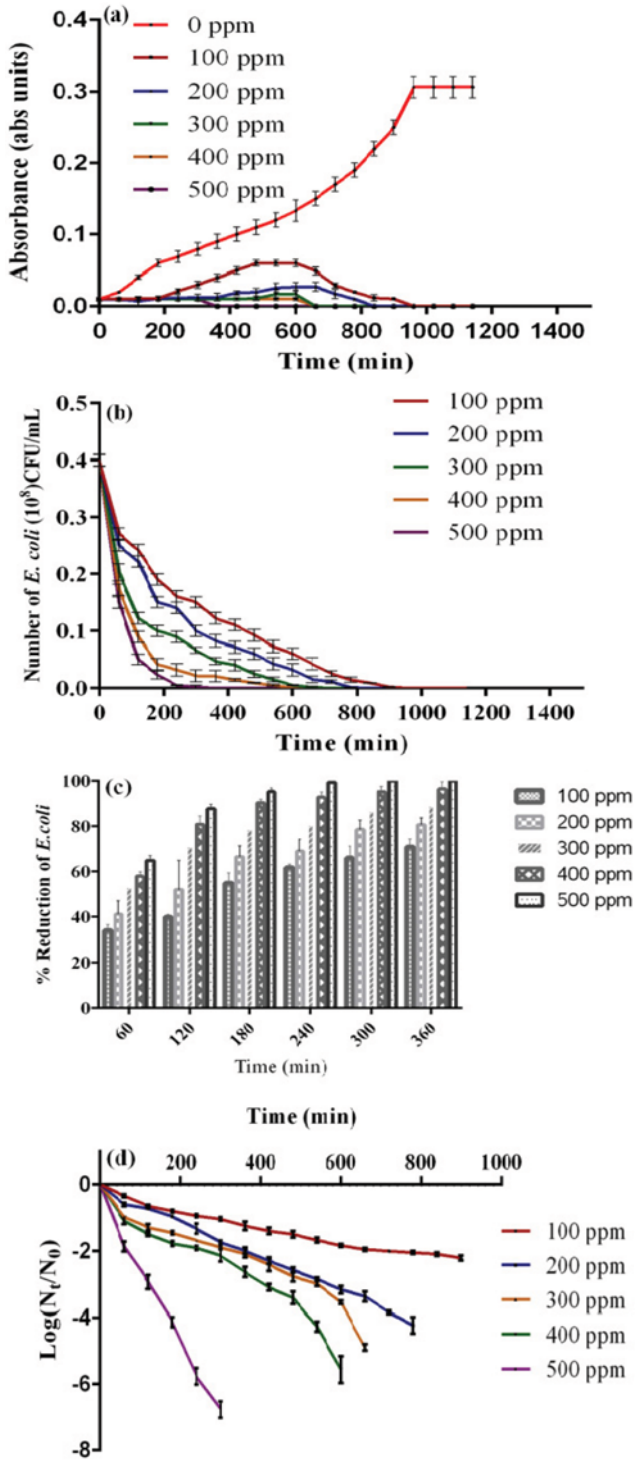

Fig. 5. Effect of *E. coli* in the presence of silver nanoparticle loaded silica (a) Growth pattern, (b) Inactivation, (c). Reduction percentage and (d) Log reduction.

Table 3. BET Surface area analysis of Silica, Amine functioned silica and Silver nanoparticle loaded silica

Sample	Surface area (m^2/g)	Total pore volume (cm^3/g)	Average pore diameter (nm)
Silica	406	0.567	14
Amine functionalized silica	280	0.450	12
Silver nanoparticles loaded silica	268.87	0.430	11.2

silica.

The physical changes of the silica by the functionalization of 3-APTES (3-Amino Propyl Tri Ethoxy Silane) and the loading of silver nanoparticle were analyzed by BET surface area analysis. Table 3 shows the BET surface area for silica was 406 m^2/g and the pore volume of 0.567 cm^3/g. The amine functionalized silica showed decreased surface area of 280 m^2/g, due to the filling of pores by the 3-APTES radicals (Li et al., 2010). Silver nanoparticle loaded silica showed further decreased surface area of 268.87 m^2/g and pore volume 0.430 cm^3/g. These results confirmed the silver nanoparticle loaded on silica surfaces.

2. *E. coli* NCIM 2685 Growth Inhibition Studies

The growth curves of *E. coli* NCIM 2685 treated with silver nanoparticle loaded silica at various concentration of 100 to 500 ppm waweres measured at OD_{600} as shown in Fig. 5(a). The growth of *E. coli* in the control experiment was observed with three distinct growth phases of lag, exponential and stationary phases. Whereas, in the presence of 100, 200 and 300 ppm of silver nanoparticle loaded silica treated *E. coli* cells were observed with prolonged lag phase and the growth was lagged to 180, 360 and 450 min, respectively. At lower concentrations of silver nanoparticle loaded silica treated *E. coli* cells took time for adaptation to the environment, but they do not have enough to outpace for reproduction, hence the growth was inhibited [23]. Complete growth inhibition of *E. coli* cells was achieved in 400 and 500 ppm of silver nanoparticle loaded silica.

Fig. 5(b) shows the inactivation of ~10^8 colony forming units (CFU/mL) of *E. coli* NCIM 2685 by silver nanoparticle loaded silica with different concentration (100-500 ppm) supplemented in 100 mL of LB broth. The number of viable cells after treatment with 100, 200, 300 and 400 ppm concentration showed the decreased CFU/mL from 10^7 to 10^5, 10^4, 10^3 and 10^2 CFU/mL, respectively. Complete inhibition of *E. coli* was observed at 500 ppm. Complete inhibition of growth of *E. coli* depends on the incubation time; the lowest concentration of 100 ppm of silver nanoparticle loaded silica was at 900 min, while increasing concentration of 200, 300, 400 and 500 ppm showed complete inactivation at 780, 660, 600 and 300 min, respectively. The results indicate that the initial CFU/mL depends on the inoculum size, and further inhibition depends upon the concentration of silver nanoparticle loaded silica and contact time [24].

Fig. 5(c) shows the percentage reduction of *E. coli* NCIM 2685 after treatment with different concentration of silver nanoparticle loaded silica from 100-500 ppm at varying time ranges from 60-360 min at the interval of 60 min. The results show that the maximum percentage reduction of *E. coli* cells after treatment of 360 min was observed to be increased as 70, 81, 89, 96 and 100% with an increase of silver nanoparticle loaded silica concentration of 100, 200, 300 400 and 500 ppm. Such inactivation studies using graphite oxide composite at different concentration from 0.1 to 1.5 mol/L were reported as effective filter and achieved complete inactivation after 24 h of treatment [25].

Fig. 5(d) shows the log reduction of *E. coli* cells after the treatment with silver nanoparticle loaded silica in different concentration from 100-500 ppm. The maximum of 2.2 and 4.2 $\log_{10}$ reduction was observed in the concentration of 100 and 200 ppm at a contact time of 900 and 780 min. The increased concentration was observed with 4.9 and 5.5 $\log_{10}$ reduction in the concentration of 300 and 400 ppm of silver nanoparticle loaded silica. Maximum inactivation (99.9%) with a 6.8 $\log_{10}$ reduction was observed for 500 ppm concentration of silver nanoparticle loaded silica at 300 min. Similar inactivation of *E. coli* was reported with 4 $\log_{10}$ reduction for chlorine disinfection [26]. Previous studies reported such inactivation studies against 10^6 of *S. aureus* showing 5 $\log_{10}$ CFU/mL reduction using 0.2 ppm of silver nanoparticle at 90 min. Whereas, a decrease of inoculum size into 10^5 was reported with the complete inactivation at the earliest of 30 min. Thus, a longer treatment time has a positive effect on bacterial inactivation [26]. These results confirm that the silver nanoparticle loaded silica can be used as an efficient adsorbent.

These results confirm that a higher initial concentration of silver nanoparticle loaded silica shows better inactivation efficiency on *E. coli* NCIM 2685. The bacterial inactivation was analyzed using inactivation kinetics models, Chick, Chick-Watson and Homs using MATLAB [27].

2-1. Inactivation Kinetic Models

The inactivation kinetic models were used to idealize the complex phenomenon of disinfection. The simple kinetic model proposed by Chick indicates the close similarity of microbial inactivation rate and their interaction. Watson developed an empirical logarithmic function to relate the inactivation rate with the disinfectant concentration. The dilution coefficient value of the Chick-Watson model, n close to unity indicated the fixed value of concentration and contact time resulted in a fixed degree of inactivation [28]. Homs model describes the relationship between disinfectant concentration, contact time and empirical constants of m (order of the reaction) and n (dilution constant). If the m value is equal to unity, then the model gets reduced to Chick-Watson model. According to the m values the type of inactivation has been analyzed; if the m value is greater than 1, this indicates the shoulder or lag curve of inactivation. An m value of less than 1 indicates the tailing curve of inactivation [26]. The inactivation kinetic plots of Log (N_t/N_0) against time (C_t) for Chick, Chick-Watson and Homs models are shown in Fig. 6.

The Chick inactivation rate constant (k) was found to be increased from 0.013-0.032 min^{-1} with the increased concentration of silver nanoparticle loaded silica from 100-500 ppm. The Chick model fitted well with the experimental data with significant R^2> 0.9 (Fig. 6(a)). This indicated that the growth of *E. coli* NCIM 2685 increases with increasing concentration of silver nanoparticle loaded silica.

The Chick-Watson kinetic model was observed with the n values closer to unity, as shown in Table 2, hence fixed degree of inactivation was achieved at a fixed concentration of silver nanoparticle loaded silica at a fixed time [28]. Fig. 6(b) shows Chick-Watson inactivation rate constant k′ values ranging from 0.012-0.019 min^{-1} with significant R^2 values (>0.9). Similar disinfectant studies were reported with the inactivation kinetic constant rate of 0.036 using silver modified TiO_2 nanotube arrays [29].

The Homs model describes the type of inactivation. Fig. 6(c) shows lower dilution coefficient values (n<1), signifying that the contact time proceeded over the concentration of the silver nano-

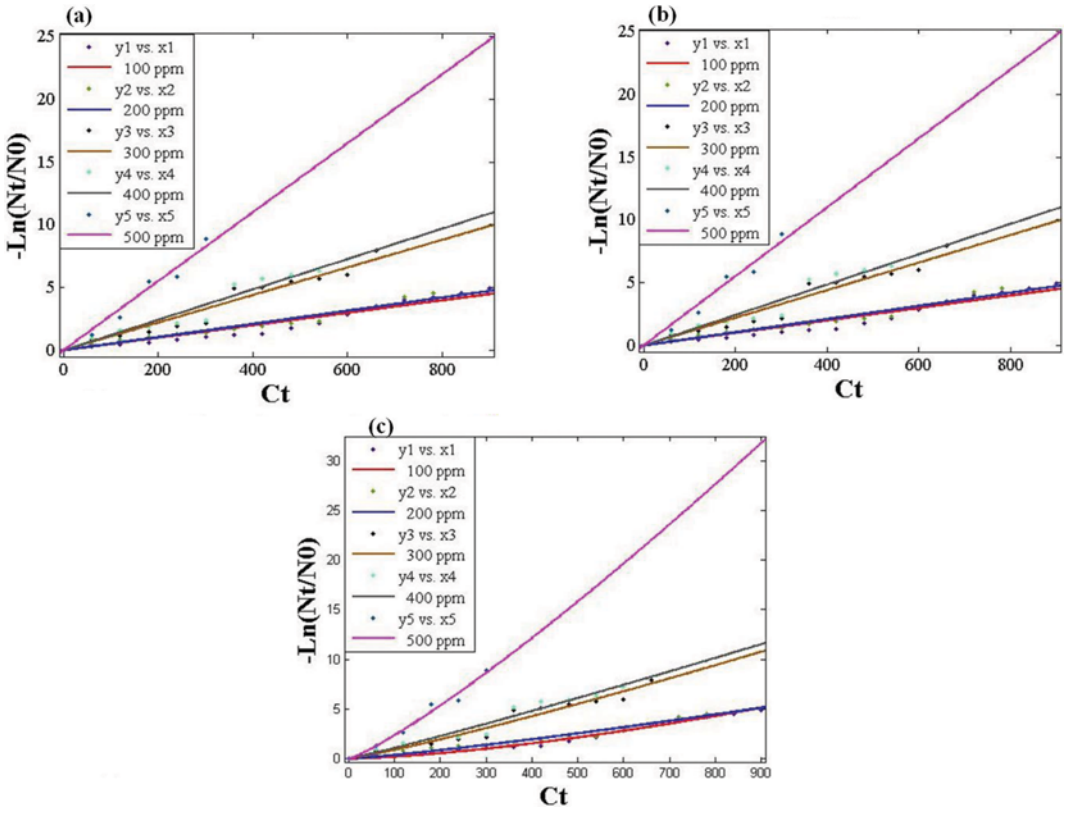

Fig. 6. Inactivation kinetic models using silver nanoparticle loaded silica against *E. coli* (a) Chicks (b) Chick-Watson and (c) Homs.

Table 4. Bacterial inactivation kinetics of silver nanoparticle loaded silica

Bacterial inactivation kinetics		Silver nanoparticle loaded silica (ppm)				
Models	Parameters	100	200	300	400	500
Chick	k (min^{-1})	0.013	0.014	0.015	0.022	0.032
	R^2	0.965	0.939	0.946	0.955	0.969
Chick-Watson	k′ (min^{-1})	0.012	0.013	0.014	0.015	0.019
	n	0.757	0.988	0.941	0.630	0.899
	R^2	0.965	0.939	0.946	0.955	0.969
Homs	k′ (min^{-1})	0.004	0.008	0.015	0.016	0.022
	m	1.13	1.17	1.32	1.09	0.97
	n	0.056	0.132	0.056	0.052	0.317
	R^2	0.976	0.938	0.946	0.954	0.956

particle loaded silica. The m values were observed to be above and closer to unity, hence the shoulder or lag curve of inactivation was described with significant R^2 values (>0.9) [30].

The results showed that the Homs model fitted well with the experimental data and indicated the type of inactivation, hence the *E. coli* inactivation was successfully described using Homs model (Table 4).

3. Batch Adsorption Studies

3-1. Effect of Silver Nanoparticle Loaded Silica on COD Removal

The effects of silver nanoparticle loaded silica from 20-80 g on COD removal from 1,000 mL of raw tannery, dairy and canteen effluent with initial COD of 5,600 mg/L, 8,000 mg/L and 3,200 mg/L at room temperature are shown in Fig. 7(a).

The results show the increased COD reduction from 17 to 73% with an increase in adsorbent dosage from 20-80 g for tannery effluent. Increased COD reduction from 26 to 83% and 37 to 93% with the increasing adsorbent dosage from 20 to 80 g for dairy effluent and canteen effluent. Further increase in adsorbent dose from 80 g to 100 g did not influence the COD removal from canteen effluent, while there was a significant COD removal of 81 and 87% from tannery and dairy effluents.

The results show an increased COD removal with an increase in adsorbent dosage. This might be due to increased number of active sites in the adsorbent surface. Calvete et al. [31] reported such substantial increase in COD removal percentage of industrial wastewater using activated carbon from agricultural byproducts

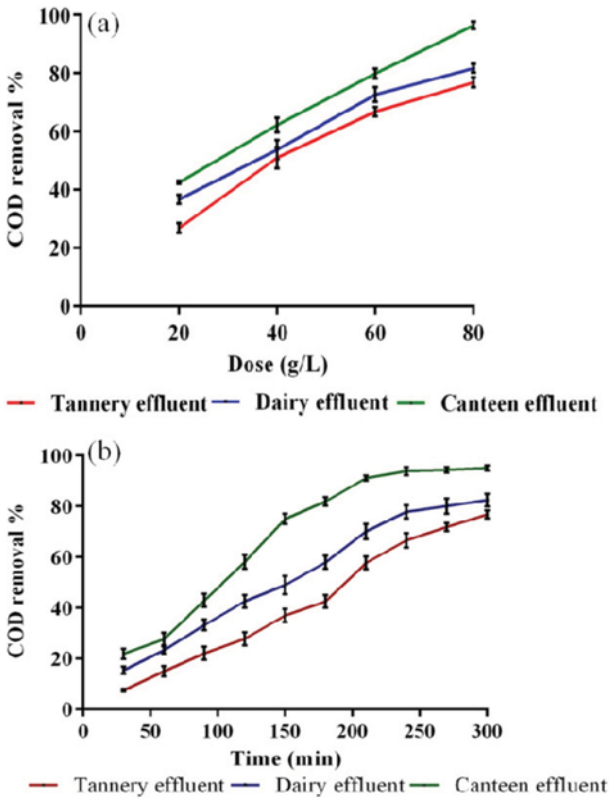

Fig. 7. Effect of silver nanoparticle loaded silica on COD removal by (a) Dosage of silver nanoparticle loaded silica and (b) contact time.

with the increased dosage from 10 g to 20 g. Equilibrium saturation of adsorbent was due to partial aggregation among the available active binding sites present in the adsorbent, and may be due to absence of pollutants to interact with adsorbent [32].

3-2. Effect of Contact Time on COD Removal

The effects of contact time on COD removal from tannery, dairy and canteen effluents were studied from 60 to 300 min with 80 g of silver nanoparticle loaded silica. Fig. 7(b) shows the COD removal capability of silver nanoparticle loaded silica increased with increase in time up to 300 min, and thereafter no significant change in the rate of COD removal was observed. The COD reduction was increased with increase in time and reached a maximum removal of 77, 82 and 97 for tannery, dairy and canteen effluents at 300 min. Such rapid reduction of COD during the initial time period may be due to the availability of more active sites in the adsorbent [19].

3-3. Adsorption Isotherm

The COD removal efficiency of silver nanoparticle loaded silica was analyzed by plotting the experimental data using the isotherm models of Langmuir, Freundlich, Redlich-Peterson and Sips isotherm models. The non-linear plot of specific adsorption (q_e) against the equilibrium concentration (C_e) for dairy, tannery and canteen effluents is shown in Fig. 8(a), (b) and (c), and their parameter values are shown in Table 5.

The Langmuir isotherm for silver nanoparticle loaded silica was observed with the maximum adsorption capacity of 145, 142 and

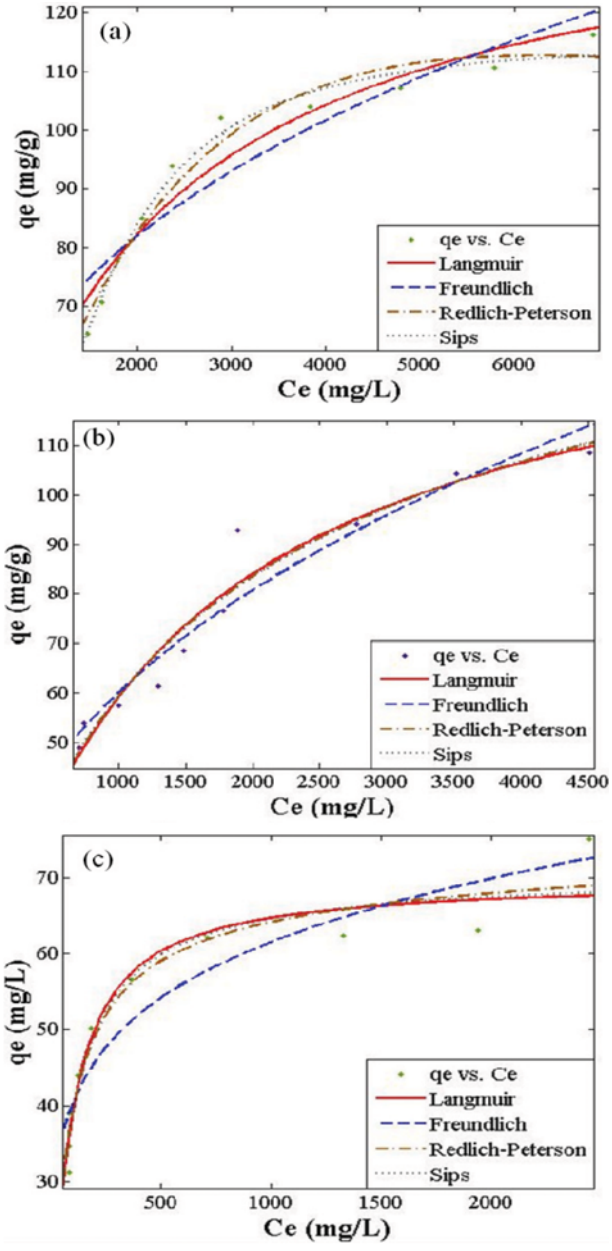

Fig. 8. Nonlinear isotherm for COD removal efficiency of silver nanoparticle loaded silica for (a) dairy effluent, (b) tannery effluent and (c) canteen effluent.

69 mg/g for tannery, dairy and canteen effluents. The R^2 values of above 0.9 were found to be significant, and the results fitted well with the experimental data (Fig. 8). The results show the Langmuir isotherm with increased q_e values with increased adsorbent dosage from 20-80 g/L. The b values (Langmuir binding constant) were decreased with increased initial COD concentration as 0.0006, 0.0006 and 0.0012 for tannery, dairy and canteen effluents, respectively. The dimensionless constant of the Langmuir isotherm (R_L) calculated from Eq. (3) as given below was less than unity, and was 0.17, 0.017 and 0.02 for tannery, dairy and canteen effluents. The results indicate a favorable adsorption process [33]. Low et al. [32] reported the increased q_e values with an increase of adsorbent

Table 5. Adsorption isotherm model and its parameter values

Isotherm model	Parameters	Effluents		
		Tannery	Dairy	Canteen
Langmuir	q_0 (mg/g)	145	142	69
	b (L/mg)	0.0006	0.0006	0.012
	R_L	0.172	0.0172	0.02
	R^2	0.940	0.945	0.934
Freundlich	k_F (mg/g)(L/mg)$^{1/n}$	3.2	7.67	17.2
	n	2.35	3.21	5.42
	R^2	0.882	0.933	0.887
Redlich-Peterson	α_R (mg/L)$^{\beta}$	0.009	0.0098	0.02
	β	0.92	0.93	0.95
	k_R (L/mg)	1.3	1.2	1.05
	R^2	0.968	0.946	0.938
Sips	k_S (L/mg)$^{1/n}$	0.0004	0.0013	0.017
	n	0.994	0.967	0.943
	q_m (mg/g)	145	142	69
	R^2	0.986	0.946	0.935

dose for COD removal [34]. An increased concentration of pollutant was observed with decreased maximum adsorption capacity [32]. This is in line with the present study, and the q_e values were decreased with increased COD values in order of tannery<dairy< canteen effluent.

$$R_L = \frac{1}{1+bC_0} \quad (3)$$

The Freundlich isotherm constant (k_F) for silver nanoparticle loaded silica was decreased with an increase of initial COD in the order of tannery>dairy>canteen effluents. The R^2 values were significant and greater than 0.88, 0.93 and 0.88 for tannery, dairy and canteen effluents, respectively. The Freundlich exponent value (1/n) was 0.31, 0.42 and 0.18 for tannery, dairy and canteen effluents, which was below 1 so indicates the normal Langmuir isotherm [34]. Freundlich isotherm was suitable for different adsorbate species and suitable for a real aquatic environment [18].

The Redlich-Peterson exponent β value for silver nanoparticle loaded silica was 0.968, 0.946 and 0.938 for tannery, dairy and canteen effluents, respectively, hence the data preferably fitted to the Langmuir model. The β value is the rate limiting behavior of the model; if β value is 1, it indicates the Langmuir form; if β value is 0, it indicates the Henry's form [32]. Studies have reported that the absorption of Reactive Black 5 is well described by Redlich-Peterson isotherm, and follows the reduced Freundlich isotherm with larger β value [35]. The adsorption capacity of silver nanoparticle silica was 144, 122 and 52 mg/g for tannery, for dairy and canteen effluents.

The sips isotherm constant (k_s) values for silver nanoparticle loaded silica was 0.0004, 0.0013 and 0.0017 for tannery, dairy and canteen effluents, respectively. A favorable adsorption process was obtained with k_s values less than 1. The monolayer adsorption capacity q_m calculated using Sips model was 145, 142 and 69 mg/g for tannery, dairy and canteen effluents (Table 5). The Sips exponent (1/n) values were closer to 1, indicating the adsorption process obeys Langmuir model, for tannery, dairy and canteen effluents, respectively. Zheng et al. [36] reported the similar Langmuir adsorption of heavy metals on the corn stalk adsorbent. The COD removal of date-pit activated carbon was also reported with the Langmuir isotherm [37].

By comparing the correlation coefficient values and the experimental adsorption capacity of silver nanoparticle loaded silica, the Langmuir isotherm is more suitable for describing the COD reduction. This may be due to monolayer adsorption by surface active sites. The adsorption efficiency of silver nanoparticle loaded silica was comparatively greater than in the literature, with respect to the adsorption of silica. The silica obtained from rice husk was reported with maximum COD removal of 81.5% from tannery wastewater with initial COD of 8,256 mg/L, by treated 250 mL of sample with 15 g of silica [38]. Similarly, the rice husk containing 96.34% silica of 1 g was used for the treatment of lack water and reported with 80.77% COD removal [39].

Table 6. Kinetics and its parameter values

Kinetic models	Parameters	Tannery effluent				Dairy effluent				Canteen effluent			
	Adsorbent dosage	20 g	40 g	60 g	80 g	20 g	40 g	60 g	80 g	20 g	40 g	60 g	80 g
Zero order	K (mgL^{-1}min^{-1})	5.83	16.94	19.02	17.93	11.49	10.63	10.53	6.96	4.97	5.55	5.67	7.83
	R^2	0.695	0.911	0.852	0.839	0.895	0.810	0.714	0.681	0.840	0.794	0.744	0.816
First order	K_1 (min^{-1})	0.001	0.004	0.005	0.005	0.0035	0.0041	0.0061	0.0061	0.0027	0.0028	0.0046	0.0118
	R^2	0.741	0.873	0.905	0.912	0.893	0.862	0.814	0.862	0.892	0.871	0.886	0.897
Second order	K_2 (Lmg^{-1}min^{-1})	2×10^{-07}	1×10^{-06}	2×10^{-06}	2×10^{-06}	4×10^{-07}	1×10^{-06}	2×10^{-06}	5×10^{-06}	1×10^{-06}	2×10^{-06}	4×10^{-06}	3×10^{-05}
	R^2	0.735	0.891	0.895	0.899	0.876	0.854	0.891	0.873	0.899	0.896	0.897	0.723
Pseudo-first order	K_{1p} (min^{-1})	0.011	0.014	0.019	0.019	0.011	0.0014	0.014	0.0019	0.011	0.0013	0.013	0.014
Experimental	**q_e (mg/g)**	**123**	**101**	**78**	**61**	**74**	**70**	**55**	**50**	**64**	**39**	**35**	**30**
Theoretical	**q_e (mg/g)**	**123**	**109**	**79**	**63**	**79**	**63**	**50**	**45**	**63**	**39**	**35**	**31**
	R^2	**0.971**	**0.943**	**0.967**	**0.969**	**0.967**	**0.996**	**0.998**	**0.955**	**0.981**	**0.996**	**0.993**	**0.998**
Pseudo-second order	K_{2p} (g mg^{-1} min^{-1}) 10^{-06}	0.8	0.03	0.02	0.01	0.01	0.01	0.01	0.006	1.2	0.5	0.3	0.3
	q_e (mg/g)	185	175	166	138	125	111	100	83	100	77	59	57
	R^2	0.915	0.871	0.839	0.891	0.506	0.792	0.794	0.886	0.394	0.950	0.966	0.938

3-4. Adsorption Kinetic Models

Five different kinetic models, namely zero-order, first-order, second-order, pseudo-first-order and pseudo-second-order were applied to experimental data to analyze the COD removal efficiencies at a time interval of 60-300 min. The significance of the adsorption process was evaluated based on the parameter values from the linearized graph and the R^2 values.

The results reveal that the zero-order, first-order, second-order linear kinetic graphs showed a poor fit to the experimental data with less R^2 values, as summarized in Table 6. The adsorption process depends on adsorbent dosage and adsorbate; hence, the zero-order kinetics was not significant for the adsorption process [40]. The pseudo-second order kinetic plot t/qt Vs. t for silver nanoparticle loaded silica was observed with poor fit to the experimental data.

Fig. 9 shows the pseudo-first-order linear plot for Log ($q_e - q_t$) Vs. Time (min) for silver nanoparticle loaded silica. The maximum adsorption capacity and the R^2 values for pseudo-first-order kinetic model fitted well to the experimental data. This may be due to COD removal from adsorbate through porous silver nanoparticle loaded adsorbents and boundary layer adsorption through pore diffusion. Similar monolayer adsorption using activated carbon was reported for phenol removal from aqueous solution which obeys pseudo-first-order kinetics [41]. The adsorption of methylene blue dye using beach sand was reported with pseudo-first-order kinetics [42]. Agricultural residues such as chaff, rice husk, sesame husk, sun flower husk and tea waste are reported for lead removal and described by pseudo-first-order kinetics [43]. The present study of COD removal obeys pseudo-first-order; this may be due to the surface adsorption of pollutants by the hydroxyl and carbonyl groups of silver nanoparticle loaded silica.

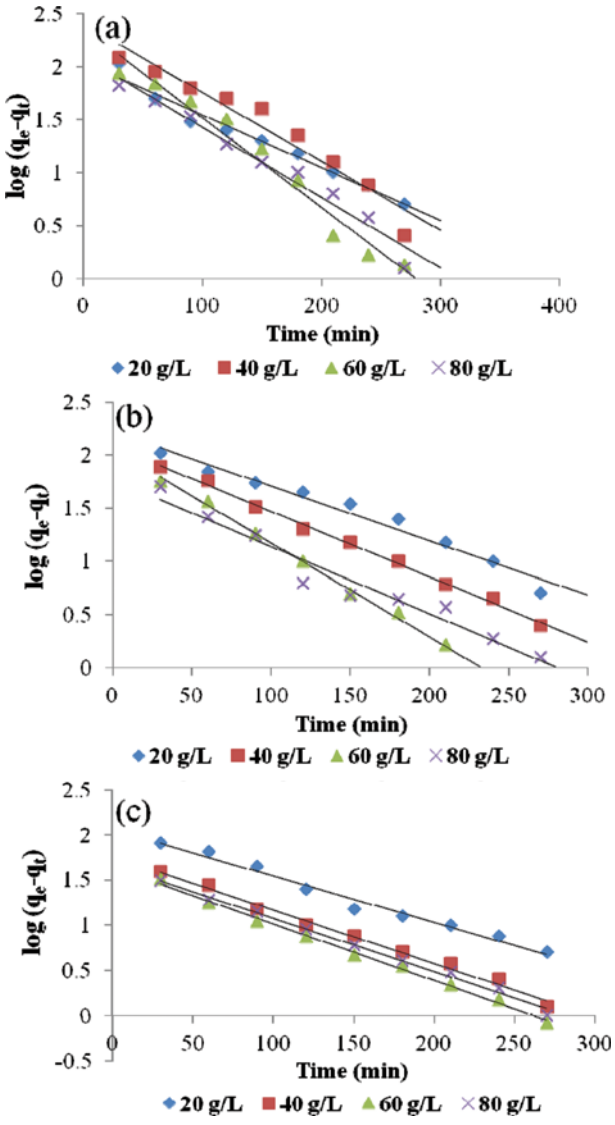

Fig. 9. Kinetic models for COD removal by silver nanoparticle loaded silica, Pseudo-first order kinetics for (a) tannery, (b) dairy, and (c) canteen effluents.

4. Reusability of Silver Nanoparticle Loaded Silica

The treated effluent samples analyzed by inductively coupled plasma optical emission spectrometry (ICP-OES) analysis were observed with nondetectable amount of silver traces. This indicates the silver nanoparticle loaded silica was stable and could be reused. The used spent adsorbent was washed with 0.5, 0.1 and 0.15 M NaOH, and the reuse of the regenerated adsorbent for COD removal is shown in Table 7.

The regenerated silver nanoparticle loaded silica followed by washing with 0.15 M NaOH showed the maximum percentage of COD removal 65, 60 and 55% for cycle 1, cycle 2 and cycle 3 from tannery effluent. For dairy effluent treatment the regenerated silver nanoparticle loaded silica showed 75, 70 and 60% COD removal for cycle 1, cycle 2 and cycle 3. For canteen effluent treatment the regenerated silver nanoparticle loaded silica showed 80, 75 and 70% COD removal for cycle 1, cycle 2 and cycle 3, respectively. The regenerated silver nanoparticle loaded silica was efficient in COD removal for up to three cycles. This indicates that the prepared adsorbent is cost-effective and prominent.

The growth inhibition by silver nanoparticle loaded silica was confirmed by the pour plate technique in that there were no colonies observed for *E. coli*. Similarly, the regenerated spent adsorbents for cycle 1, cycle 2, cycle 3 supplemented petri plates were no colonies for *E. coli*. Whereas, in the control experiment, silica

Table 7. COD removal percentage of regenerated silver nanoparticle loaded silica

Tannery effluent		0.05	0.1	0.15
COD removal %	Cycle 1	60	62	**65**
	Cycle 2	55	57	**60**
	Cycle 3	50	52	**55**
Dairy effluent				
COD removal %	Cycle 1	70	73	**75**
	Cycle 2	65	67	**70**
	Cycle 3	55	58	**60**
Canteen effluent				
COD removal %	Cycle 1	75	77	**80**
	Cycle 2	70	72	**75**
	Cycle 3	60	65	**70**

supplemented petri plate showed the normal *E. coli* growth (~10^{-5}). These results show that the prepared adsorbent and the regenerated spent adsorbent has potential against *E. coli* upto 3 cycles.

CONCLUSIONS

An attempt has been made to prepare a potential, ecofriendly and low cost absorbent to treat industrial effluent. The inactivation of *E. coli* using the prepared adsorbent obeys Homs model. The inactivation rate constant was 0.022 min^{-1} with significant R^2 value of 0.956. The batch adsorption studies for COD removal from tannery, dairy and canteen effluent using the prepared adsorbent were significant and follow Langmuir isotherm of physisorption with maximum adsorption capacity of 145, 142 and 69 mg/g for tannery, dairy and canteen effluents. The kinetic model fitted well with the experimental values and were described well using pseudo-first order kinetics. These results indicate that silver nanoparticle loaded silica provides an alternative and potential adsorbent for the treatment of industrial effluents. The silver nanoparticle loaded silica is also affordable by the small scale industries that reduces the discharge of untreated wastewater and thus eradicate the waterborne diseases.

CONFLICT OF INTEREST

The authors have declared no conflict of interest.

NOMENCLATURE

N_0 : initial concentration of *E. coli* [m^{-3}]
N_t : concentration of *E. coli* at time t [m^{-3}]
k : first order inactivation rate constant [s^{-1}]
k′ : pseudo first order inactivation rate constant [s^{-1}]
C_e : equilibrium concentration [mg/L]
C_0 : initial concentration [mg/L]
q_e : equilibrium concentration [mg/g]
q_0 : maximum adsorption capacity [mg/g]
b : Langmuir binding constant
R_L : dimensionless separation factor
k_F : Freundlich constant [(mg/g)(L/mg)^n]
n : heterogeneity factor
k_R : Redlich-Peterson constants [L/mg]
α_R : Redlich-Peterson constants [mg/L]$^{-\beta}$
β : Redlich-Peterson isotherm exponent
k_S : sips isotherm constant [mg/L]$^{-(1/n)}$
q_m : monolayer capacity [mg/g]
(1/n) : sips isotherm exponent
K : rate constant [$mgL^{-1}min^{-1}$]
C_i : initial concentration of pollutant [mg/L]
C_t : concentration of pollutant [mg/L] at time t
K_1 : rate constant of first order [min^{-1}]
K_2 : rate constant of second order [L mg^{-1} min^{-1}]
q_e : final COD concentration at equilibrium [mg/g]
q_t : final COD concentration at time t [min]
K_{1p} : pseudo-first order kinetic constant [min^{-1}]
K_{2p} : pseudo-second order kinetic constant [g mg^{-1} min^{-1}]
α : initial adsorption rate constant [mg g^{-1} min^{-1}]
β : monolayer coverage of the adsorbent [g mg^{-1}]

SUPPORTING INFORMATION

Additional information as noted in the text. This information is available via the Internet at http://www.springer.com/chemistry/journal/11814.

REFERENCES

1. Jaishree and T. I. Khan, *Int. J. Scientific Res. Publication*, **4**(3), 1 (2014).
2. H. Ozgun, M. E. Ersahin, S. Erdem, B. Atay, S. Sayili, E. Eren, P. Hoshan, D. Atay, M. Altinbas, C. Kinaci and I. Koyuncu, *Clean - Soil, Air, Water*, **41**(12), 1175 (2013).
3. F. Rahmawati, T. Kusumaningsih and A. Hastuti, *Toxicological Environ. Chem.*, **93**(8), 1602 (2011).
4. M. H. El Rafie, T. I. Shaheen, A. A. Mohamed and A. Hebeish, *Carbohydr. Polym.*, **90**, 915 (2012).
5. M. Rai and C. Posten, Green Biosynthesis of Nanoparticles Mechanisms and Applications, CABI Publishers, UK (2013).
6. F. Okafor, A. Janen, T. Kukhtareva, V. Edwards and M. Curley, *Int. J. Environ. Res. Public Health*, **10**, 5221 (2013).
7. Y. Lv, H. Liu, Z. Wang, S. Liu, L. Hao, Y. Sang, D. Liu, J. Wang and R. I. Boughton, *J. Memb. Sci.*, **331**, 50 (2009).
8. J. Pal, M. K. Deb, D. K. Deshmukh and D. Verma, *Appl. Water Sci.*, **3**, 367 (2013).
9. K. Vimala, Y. M. Mohan, K. Varaprasad, N. Narayana Reddy, S. Ravindra, N. Sudhakar Naidu and K. M. Raju, *J. Biomater. Nanobiotechnol.*, **2**, 55 (2011).
10. T. Q. Tuan, N. V. Son, H. T. K. Dung, N. H. Luong, B. T. Thuy, N. T. V. Anh, N. D. Hoa and N. H. Hai, *J. Hazard. Mater.*, **192**, 1321 (2011).
11. N. R. Jana, C. Earhart and J. Y. Ying, *Chem. Mater.*, **19**, 5074 (2007).
12. F. Li, P. Du, W. Chen and S. Zhang, *Anal. Chim. Acta*, **585**, 211 (2007).
13. G. Compagnini, M. E. Fragala, L. D. DUrso, C. Spinella and O. Puglisi, *J. Mater. Res.*, **16**, 2934 (2001).
14. D. V. Quang, P. B. Sara Wade, A. Hilonga, S. D. Park, J. K. Kim and H. T. Kim, *Appl. Surf. Sci.*, **257**, 4250 (2011).
15. V. Thamilselvi and K. V. Radha, *Dig. J. Nanomater Bios.*, **8**, 1101 (2013).
16. H. Chick, *J. Hygiene*, **8**, 92 (1908).
17. D. Eaton, L. S. Clesceri, A. E. Greenberg and M. A. H. Franson,. American Public Health Association, 19th Ed. Washington (1995) DC.
18. S. Aber and M. Sheydaei, *Clean - Soil, Air, Water*, **40**(1), 87 (2012).
19. Y. P. Teoh, M. A. Khan and T. S. Y. Choong, *Chem. Eng. J.*, **217**, 248 (2013).
20. A. B. Dos Santos, F. J. Cervantes and J. B. Van Lier, *Bioresour. Technol.*, **98**(12), 2369 (2007).
21. E. Sumesh, M. S. Bootharaju, Anshup and T. Pradeep, *J. Hazard. Mater.*, **189**, 450 (2011).
22. S. K. Das, M. M. R. Khan, T. Parandhaman, F. Laffir, A. K. Guha,

G. Sekarana and A. B. Mandal, *Nanoscale*, **5**, 5549 (2014).
23. W. R. Li, X. B. Xie, Q. S. Shi, H. Y. Zeng, Y. S. OU-Yang and Y. B. Chen, *Appl. Microbiol. Biotechnol.*, **85**, 1115 (2010).
24. P. Jain and T. Pradeep, *Biotechnol. Bioeng.*, **90**, 59 (2005).
25. W. H. Jung, H. C. Koo, K. W. Kim, S. Shin, S. H. Kim and Y. H. Park, *Appl. Environ. Microbiol.*, **74**(7), 2171 (2008).
26. Y. J. Lee and S. H. Nam, *J. Microbiol.*, **40**, 119 (2002).
27. I. Sheet, H. Holail, Z. Olama, A. Kabbani and M. Hines, *Int. J. Current Microbiol. Appl. Sci.*, **2**(4), 1 (2013).
28. S. B. Somani and N. W. Ingole, *Int. J. Environ. Sci.*, **2**, 1344 (2012).
29. L. T. Kist, C. Albrecht and E. L. Machado, Clean-soil, Air, Water, **36**(9), 775 (2008).
30. A. L. Jessen, ProQuest, Ann Arbor, U.S.A. (2006).
31. T. Calvete, E. C. Lima, N. F. Cardoso, S. L. P. Dias and E. S. Ribeir, *Clean - Soil, Air, Water*, **38**, 521 (2010).
32. L. W. Low, T. T. Teng, A. Ahmad, N. Morad and Y. S. Wong, *Water Air Soil Pollution*, **218**, 293 (2011).
33. D. Mohan, K. P. Singh and V. K. Singh, *J. Hazard. Mater.*, **152**(3), 1045 (2008).
34. A. A. Ahmad and B. H. Hameed, *J. Hazard. Mater.*, **172**, 1538 (2009).
35. R. Liu, X. Shen, X. Yang, Q. Wang and F. Yang, *J. Nanopart. Res.*, **15**, 1679 (2013).
36. L. Zheng, Z. Dang, X. Yi and H. Zhang, *J. Hazard. Mater.*, **176**, 650 (2010).
37. M. H. El-Nass, S. Al-Zuhair and M. A. Ahaija, *J. Hazard. Mater.*, **173**, 1750 (2010).
38. D. Sivakumar, *Global J. Environ. Sci. Manage.*, **1**(1), 27 (2015).
39. A. A. NurFatinah, N. Rajesh and M. Z. Masniroszaime, *J. Eng. Sci. Technol.*, **1**, 8 (2015).
40. J. M. Mendez-Conteras, J. Atenodoro, F. A. Champion, N. A. Vallejo-Cantu and A. Alvardo-Lassman, *Water SA.*, **35**(4), 371 (2009).
41. S. M. Al-Hakami, A. B. Khalil, T. Laoui and M. Ali Atieh, *Bioinorg Chem. Appl.*, **2013**, 1 (2013).
42. R. Ansari, A. Mohammad-khah and M. Nazmi, *Current Chem. Lett.*, **2**, 215 (2013).
43. K. M. S. Surchi, *Int. J. Chem.*, **3**(3), 103 (2011).
44. H. E. Watson, *J. Hygiene*, **536**, 536 (1908).
45. L. W. Hom, *Journal of the Sanitary Engineering Division, ASCE*, **98**, 183 (1972).
46. I. Langmuir, *J. Am. Chem. Soc.*, **38**(11), 2221 (1916).
47. H. M. F. Freundlich, *J. Phys. Chem.*, **57**, 385 (1906).
48. O. Redlich and D. L. Peterson, *J. Phys. Chem.*, **63**, 1024 (1959).
49. R. Sips, *J. Chem. Phys.*, **16**, 490 (1948).
50. A. S. Thajeel, *Aqua. Sci. Technol.*, **1**, 53 (2013).
51. S. Idris, J. Yisa, A. U. Itodo and K. A. Popoola, *Resource and Environment*, **2**(2), 51 (2012).
52. A. H. Pakiari and Z. Jamshidi, *J. Phys. Chem. A*, **111**(20), 4391 (2007).
53. F. X. Schmid, Biological Macromolecules:UV-visible Spectrophotometry, Macmillan Publishers Ltd., Nature Publishing Group, Germany (2001).
54. S. D. Solomon, M. Bahadory, A. V. Jeyarajasingam, S. A. Rutkowsky and C. Boritz, *J. Chem. Ed.*, **84**(2), 322 (2007).